International Journal of Electrical, Electronic and Communication Sciences
ISSN: 2517-9438
Vol:8, No:8, 2014

Active Disturbance Rejection Control for Wind System Based On a DFIG

R. Chakib, A. Essadki, M. Cherkaoui

Abstract**—**This paper proposes the study of a robust control of the doubly fed induction generator (DFIG) used in a wind energy production. The proposed control is based on the linear active disturbance rejection control (ADRC) and it is applied to the control currents rotor of the DFIG, the DC bus voltage and active and reactive power exchanged between the DFIG and the network. The system under study and the proposed control are simulated using MATLAB/SIMULINK.

Keywords**—**Doubly fed induction generator DFIG, Active disturbance rejection control ADRC, Vector control, MPPT, Extended state observer, back to back converter, Wind turbine.

I. Introduction

SUSTAINABLE development and renewable energy today are of interest to several research teams. Thus, the development of wind represents a great investment in the field of technological research. The wind system that uses doubly fed induction generator and a back to back converter that connects the rotor of the generator to the grid has several advantages [1]. One advantage of this structure is that the power converters used are sized to pass a fraction of the total power of the system, which allows the reduction of losses in power electronics components [1], [14].

The system studied is a chain of wind conversion three-bladed horizontal axis using a double-fed asynchronous generator directly connected to the grid and driven by the rotor by means of the two power converters operating in PWM. These PWM converters are used to adjust the rotational speed of the generator to the wind speed to extract maximum power generated [2], [4]. (Fig. 1)

In this study, the control of the DFIG is based on three functions:

- The extraction of maximum power point tracking (MPPT)
- Vector control of DFIG with stator flux orientation according to the axis d.
- Control of PWM converters.

Performance of the wind system does not only depend on the DFIG but also the manner in which the two PWM converters are controlled [4], [15].

R. Chakib and M. Cherkaoui are with Department of Electrical Engineering of Mohammedia School of Engineers (EMI), University Mohammed V, Agdal, Rabat Morocco (e-mail: RachidChakib@ research.emi.ac.ma, cherkaoui@emi.ac.ma).

A. Essadki is with Department of Electrical Engineering of ENSET of High School of Technical Education (ENSET), University Mohammed V Souissi Rabat, Morocco (e- mail: Ahmed.essadki1@gmail.com).

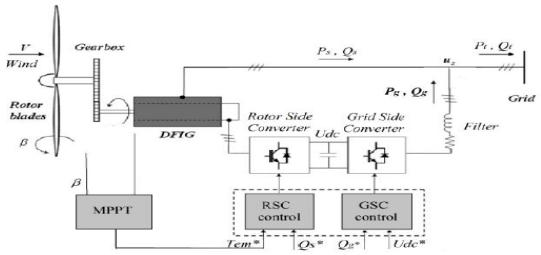

Fig. 1 Diagram of a wind turbine based on the DFIG

In this article, we present the technical control of the two converters based on active disturbance rejection control. We analyze their dynamic performance by simulations in MATLAB/SIMULINK environment.

We start by modeling of the wind turbine and the presentation of the principle of maximum extraction power. Then, we present a model of DFIG in the Park reference dq. Thereafter, we study in detail the principle and performance of the ADRC technique used in the control of rotor side converter and the grid side converter. We conclude by presenting the simulation results and their interpretation.

II. Model of Turbine and Control Strategy MPPT

A. Model of Turbine

The turbine captures kinetic energy of wind and converts it to a torque that makes rotate the rotor poles [7].

Aerodynamic power appearing at the turbine rotor is written as follows:

$$P_{aero} = \frac{1}{2} C_p(\lambda, \beta) \rho \pi R^2 v^3 \quad (1)$$

The aerodynamic torque is estimated by the following expression:

$$T_{aero} = \frac{1}{2} C_p(\lambda, \beta) \rho \pi R^2 \frac{v^3}{\Omega_t} \quad (2)$$

ρ is the air density, R is the radius of the turbine, Ωt is the turbine speed, β is the pitch angle, λ is the speed ratio and ν is the wind speed.

$$\lambda = \frac{\Omega_t . R}{v} \quad (3)$$

C_p is the power coefficient expressing the aerodynamic efficiency of the wind turbine. It depends on the speed ratio λ and the orientation angle of the blades β. C_p is intrinsic to the

constitution of the wind and depends on profiles blades [2], [8]. It can be expressed by the following relationship:

$$C_p = 0.22\left(\frac{116}{\lambda_i} - 0.4\beta - 5\right)e^{-\frac{125}{\lambda_i}} + 0.0068\lambda \quad (4)$$

where

$$\lambda_i = \frac{1}{\lambda + 0.008\beta} - \frac{0.035}{\beta^3 + 1}$$

Fig. 2 shows the curves of C_p as a function of λ for different values of β.

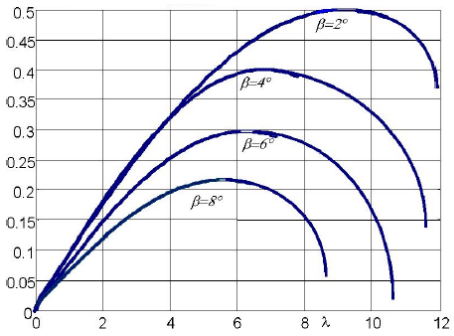

Fig. 2 Power coefficient as a function of λ et β

The mechanical speed is related to the speed of rotation of the turbine by the multiplier coefficient G. The torque on the slow axis is also related to the torque on the fast axis (generator side) by the coefficient multiplier G.

The total inertia J is consisting of turbine inertia J_t reduced on the fast axis and the inertia of the generator J_g.

$$J = \frac{J_t}{G^2} + J_g \quad (5)$$

To determine the evolution of the mechanical speed from the total torque applied to the rotor of the DFIG, we apply the fundamental equation of dynamics:

$$J\frac{d\Omega_{mec}}{dt} = T_g - T_{em} - f\Omega_{mec} \quad (6)$$

where,

T_g : Torque from the multiplier is applied to the shaft of the generator

T_{em} : The electromagnetic torque produced by the generator

$f\Omega_{mec}$: Torque of viscous friction.

The previous equations allow determining the block diagram model of the turbine Fig. 3.

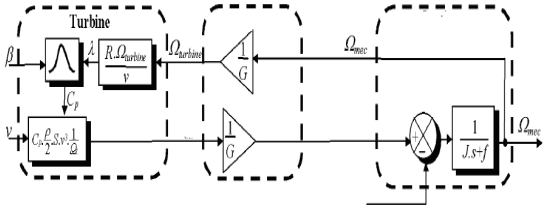

Fig. 3 Block diagram of the model turbine

B. MPPT Control Strategy

To capture maximum of the incidental energy, we must continuously adjust the rotational speed of the turbine to the wind speed [2], [9], [15]. The principle of this command is to always have a rotation of the turbine which allows a speed ratio λ=λ opt.

In this article, the turbine is controlled without speed control (Fig. 4). The electromagnetic torque reference T_{em_ref} is determined from an estimate of the wind speed and the measurement of mechanical rotation speed [2], [7].

$$T_{em\_ref} = \frac{1}{2.\lambda_{opt}^3.G} C_{pmax}\,\rho\pi R^5\Omega_t^2 \quad (7)$$

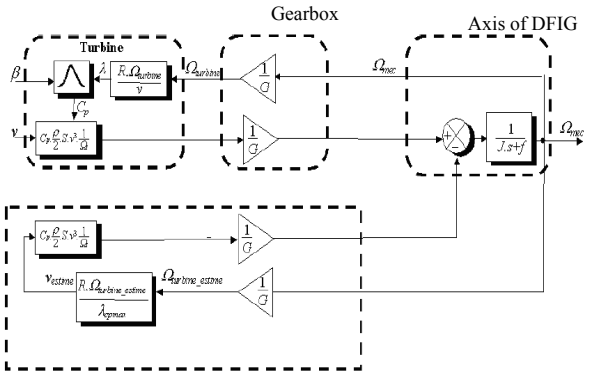

Fig. 4 Block diagram of MPPT without wind velocity measurement

III. Model of DFIG

A. Mathematical Model

Electrical equations of DFIG in the Park reference dq are given by the following expressions [6]:

$$V_{sd} = R_s\ i_{sd} + \frac{d\Phi_{sd}}{dt} - \omega_s\,\Phi_{sq} \quad (8)$$

$$V_{sq} = R_s\,i_{sq} + \frac{d\Phi_{sq}}{dt} + \omega_s\Phi_{sd} \quad (9)$$

$$V_{rd} = R_r\,i_{rd} + \frac{d\Phi_{rd}}{dt} - \omega_r\Phi_{rq} \quad (10)$$

$$V_{rq} = R_r i_{rq} + \frac{d\Phi_{rq}}{dt} + \omega_r\Phi_{rd} \quad (11)$$

$$\Phi_{sd} = L_s i_{sd} + L_m i_{rd} \quad (12)$$

$$\Phi_{sq} = L_s i_{sq} + L_m i_{rq} \quad (13)$$

$$\Phi_{rd} = L_r i_{rd} + L_m i_{sd} \quad (14)$$

$$\Phi_{rq} = L_r i_{rq} + L_m i_{sq} \quad (15)$$

The expression of electromagnetic torque:

$$T_{em} = \frac{3}{2}p\ \frac{L_m}{L_s}(i_{rd}\Phi_{sq} - i_{rq}\Phi_{sd}) \quad (16)$$

L_s is the cyclic stator inductance, L_r is the cyclic rotor inductance, L_m is mutual inductance, R_s is stator resistance,

R_r is rotor resistance , p is number of pole pairs of the generator.

Active and reactive powers stator and rotor of the DFIG are written as follows:

$$P_s = V_{sd} i_{sd} + v_{sq} i_{sq} \quad (17)$$

$$Q_s = v_{sq} i_{sd} - v_{sd} i_{sq} \quad (18)$$

$$P_r = v_{rd} i_{rd} + v_{rq} i_{rq} \quad (19)$$

$$Q_r = v_{rq} i_{rd} - v_{rd} i_{rq} \quad (20)$$

B. Vector Control Strategy

For vector control of DFIG, we chose a Park reference linked to the rotating field. By adopting the hypothesis of a stator resistance R_s as negligible [4], [15] and the stator flux Φ_s is constant and oriented along the axis d, the following equations can be deduced:

$$\Phi_{sd} = \Phi_s = L_s i_{sd} + L_m i_{rd} \quad (21)$$

$$\Phi_{sq} = L_s i_{sq} + L_m i_{rq} = 0 \quad (22)$$

$$\Phi_{rd} = \sigma L_r i_{rd} + \frac{Lm}{Ls} \Phi_{sd} \quad (23)$$

$$\Phi_{rq} = \sigma L_r i_{rq} \quad (24)$$

$$V_{sd} = R_s i_{sd} + \frac{d\Phi_{sd}}{dt} = 0 \quad (25)$$

$$V_{sq} = R_s i_{sq} + \omega_s \Phi_{sd} \simeq \omega_s \Phi_s \quad (26)$$

$$V_{rd} = R_r i_{rd} + \sigma L_r \frac{di_{rd}}{dt} - \omega_r \sigma L_r i_{rq} \quad (27)$$

$$V_{sq} = R_r i_{rq} + \sigma L_r \frac{di_{rq}}{dt} + \omega_r \sigma L_r i_{rd} + \omega_r \frac{L_m}{L_s} \Phi_s \quad (28)$$

where $\sigma = 1 - \frac{L_m^2}{L_s L_r}$: dispersion coefficient between the coilings d and q.

From (21) and (22), the stator currents can be expressed as a function of the rotor currents as follows:

$$i_{sd} = \frac{\Phi_s}{L_s} - \frac{L_m}{L_s} i_{rd} \quad (29)$$

$$i_{sq} = -\frac{L_m}{L_s} i_{rq} \quad (30)$$

The terms of active and reactive stator power can be simplified as follows:

$$P_s = -V_s \frac{L_m}{L_s} i_{rq} \quad (31)$$

$$Q_s = \frac{V_s \Phi_s}{L_s} - \frac{V_s L_m}{L_s} i_{rd} \quad (32)$$

The simplified expression for the electromagnetic torque of the DFIG is written as follows:

$$T_{em} = -\frac{3}{2} p \frac{L_m}{L_s} \Phi_s i_{rq} \quad (33)$$

The block diagram showing the simplified mathematical model of DFIG is shown in Fig. 5.

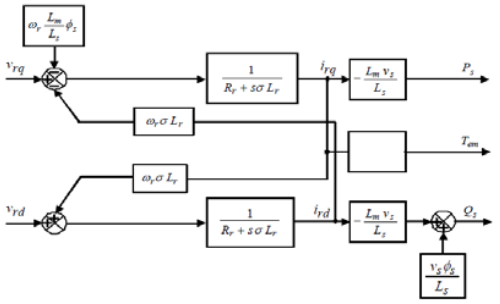

Fig. 5 Simplified model of the DFIG

V_{rd} and V_{rq} are the two-phase components of the rotor voltages to impose on the DFIG to obtain the desired rotor currents.

A judicious choice of regulators in the control loop and an adequate synthesis of these parameters will compensate the terms ($\sigma \omega_r L_r$) coupling between the two axes d and q [4], [14], [15].

IV. Back to Back Converter

The two converters of this wind turbine system (rotor side and grid side) are interconnected via a DC bus which allows for a transfer of between two sources at different frequencies. (Fig. 6)

These converters are bidirectional PWM control and they are composed of two switching cells, each is composed of two IGBT that are connected to two diode in anti-parallel.

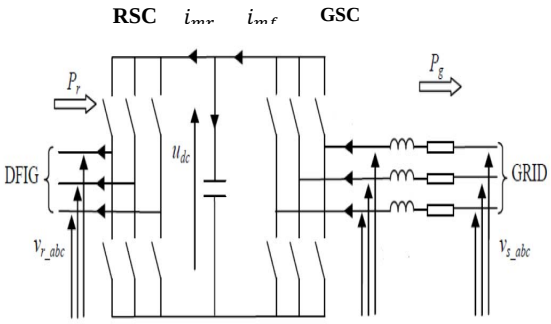

Fig. 6 Back to Back Converter

A. Rotor Side Control (RSC)

The role of the converter PWM control is to provide adequate rotor voltages to ensure the necessary torque which is used to vary the speed of the mechanical DFIG to extract the maximum power generated [4], [14].

From (33), it is clear that the electromagnetic torque T_{em} can be controlled by the rotor currents i_{rq}.

We deduce from (33):

$$i_{rq\_ref} = -\frac{2}{3}\frac{L_s}{pL_m\Phi_s}T_{em\_ref} \quad (34)$$

Substituting (7) into (34), we deduce:

$$i_{rq\_ref} = -\frac{1}{3}\frac{L_s}{pL_m\Phi_s G\lambda_{opt}^3}C_{pmax}\rho\pi R^5\Omega_t^2 \quad (35)$$

Similarly, the rotor current i_{dr} is used to control the reactive power generated Q_s. We deduce from (32):

$$i_{rd\_ref} = \frac{\Phi_s}{L_m} - \frac{L_s}{V_s L_m}Q_{s\_ref} \quad (36)$$

The simplified diagram of the control of the rotor side converter is shown in Fig. 7.

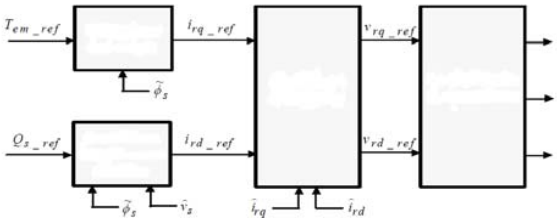

Fig. 7 Simplified diagram of the rotor side converter control

B. Grid Side Control (GSC)

This converter PWM control ensures a regulation of the DC bus voltage U_{dc} and adjusts the power factor grid side [14]-[9].

The purpose of the control of this converter is to maintain constant voltage U_{dc} and ensure unity power factor ($Q_s = 0$).

Using the dq reference, electric filter equations (R_f ,L_f) connected to the grid and the DC bus are expressed as follows:

$$L_f\frac{di_{df}}{dt} + R_f i_{df} + L_f\omega_s i_{qf} = V_{sd} - V_{df} \quad (37)$$

$$L_f\frac{di_{qf}}{dt} + R_f i_{qf} - L_f\omega_s i_{df} = V_{sq} - V_{qf} \quad (38)$$

$$V_{df} = S_{dr}U_{dc} \quad (39)$$

$$V_{qf} = S_{qr}U_{dc} \quad (40)$$

$$i_{mf} = \frac{3}{2}(S_{dr}i_{df} + S_{qr}i_{qf}) \quad (41)$$

$$C\frac{dU_{dc}}{dt} = i_{mf} - i_{mr} \quad (42)$$

S_{dr} and S_{qr} are the functions of connection switches of the grid side converter in dq referential.

The voltage V_s is oriented along the q axis, the active and reactive power grids are thus written as follows:

$$P_f = \frac{3}{2}V_{sq}i_{qf} \quad (43)$$

$$Q_f = \frac{3}{2}V_{sq}i_{df} \quad (44)$$

If we neglect losses in power converters, we obtain:

$$P_{dc} = U_{dc}i_{mf} = P_f \quad (45)$$

Substituting (42) and (43) into (45), we obtain:

$$CU_{dc}.\frac{dU_{dc}}{dt} = \frac{3}{2}V_{sq}i_{qf} - U_{dc}i_{mr} \quad (46)$$

V. Control Strategy ADRC

A. Active Disturbance Rejection Control

Active disturbance rejection control is a robust command based on the extension of the model system by a state observer to estimate what the user can not master in the mathematical model of the system to control [3], [10]. This state observer dubbed « Extended State Observer (ESO)» allows to estimate all real disturbance and modeling uncertainties [3], [5]. This estimate is used in the generation of the control signal in order to decouple the system of the disturbance acting on the actual process [3], [5], [11], [10].

This function disturbance rejection allows the user to treat the system as a simple model because the negative effects of external disturbances and modeling uncertainties are compensated for in real time [5], [12], [10], [13].

We consider the case of a first order system to illustrate the principle of the ADRC.

$$\frac{dy(t)}{dt} = -\frac{1}{T}y(t) + bu(t) \quad (47)$$

where $b = \frac{K}{T}$, $u(t)$ is the input, $y(t)$ is the output, K is the gain and T is the constant of the system.

We substitute

$$b = b_0 + \Delta b$$

where $b_0 = \frac{K}{T}$ is the known part of b, and Δb is the modeling error and/or variations in system parameters.

External disturbances are added, (47) of the system becomes:

$$\frac{dy(t)}{dt} = -\frac{1}{T}y(t) + \frac{1}{T}d(t) + \Delta bu(t) + b_0u(t)$$
$$\frac{dy(t)}{dt} = f(y,d,t) + b_0u(t) \quad (48)$$

where $f(y,d,t) = -\frac{1}{T}y(t) + \frac{1}{T}d(t) + \Delta bu(t)$ represents the total disturbance (internal and external).

The fundamental idea of the ADRC is to implement an extended state observer (ESO), which provides an estimate $\tilde{f}(t)$ such that it can compensate for the effects of $f(t)$ on the system [3], [5], [10], [12].

The description of the state space of the process described by (48) is given as follows:

$$\begin{cases} \dot{x_1} = x_2 + b_0.u \\ \dot{x_2} = \dot{f} \\ y = x_1 \end{cases} \quad (49)$$

in matrix form :

$$\begin{cases} \dot{x} = Ax + Bu + D\dot{f} \\ y = Cx \end{cases} \quad (50)$$

where $A = \begin{pmatrix} 0 & 1 \\ 0 & 0 \end{pmatrix}$, $B = \begin{pmatrix} b_0 \\ 0 \end{pmatrix}$, $C = (1 \quad 0)$ and $D = \begin{pmatrix} 0 \\ 1 \end{pmatrix}$

We cannot measure total disturbance f(t); we can only estimate using the extended state observer (ESO) built using the input u(t) and the output y(t) [3]-[5].

The equations of the extended state observer are:

$$\begin{cases} \dot{x} = Ax + Bu + D(y - \widetilde{y}) \\ \tilde{y} = Cx \end{cases} \quad (51)$$

where $D = \begin{pmatrix} \beta_1 \\ \beta_2 \end{pmatrix}$, β_1 and β_2 are the parameters of the observer. The estimated variables $\tilde{x}_1(t) = \tilde{y}$ and $\tilde{x}_2(t) = \tilde{f}(t)$ are used to implement the disturbance rejection and control laws.

$$\dot{\tilde{x}}(t) = (A - DC)\tilde{x}(t) + Bu(t) + Dy(t) \quad (52)$$

$$u(t) = \frac{u_0(t) - \tilde{f}(t)}{b_0}$$

where

$$u_0(t) = K_p(r(t) - \tilde{y}(t)) \quad (53)$$

$r(t)$ is the reference input signal to follow.

Fig. 8 shows the structure of the control loop by ADRC for a first order process [3], [5].

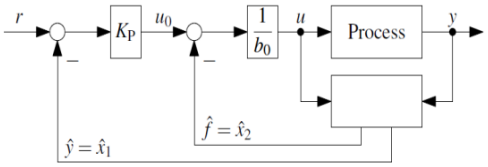

Fig. 8 ADRC topology

The gain K_p acts on the $\tilde{y}(t)$ rather than on the actual output $y(t)$. $u_0(t)$ represents the output of linear proportional controller.

By substituting (53) into (48), we show that the system behaves as a simple integrator if $f(t) = \tilde{f}(t)$.

$$\frac{dy(t)}{dt} = f(t) + b_0 \frac{u(t) - \tilde{f}(t)}{b_0} \simeq u_0(t) = K_p(r(t) - \tilde{y}(t)) \quad (54)$$

If $y(t) = \tilde{y}(t)$, behavior of order 1 is obtained in closed loop with the pole : $S_{CL} = -K_p$:

$$\frac{1}{K_p}\frac{dy(t)}{dt} + y(t) \simeq r(t) \quad (55)$$

If the state observer and disturbance rejection work properly, a proportional controller must be designed to achieve the same behavior as that of closed loop regardless of the parameters of the actual process [10], [12].

Generally, the gain K_p is chosen as a function on the desired response time of the system t_r.

$$K_p = \frac{4}{t_r} \quad (56)$$

To function correctly, the observation parameters β_1 and β_2 , defined in (51), must also be determined.

The dynamics of the observer must be fast, the poles of this observer must be placed to the left of the pole of the closed loop S_{CL} . A simple rule suggests [5]:

$$S_{ESO1} = S_{ESO2} \simeq (3 \ldots .10)S_{CL} \quad (57)$$

for the two concerned poles where $S_{CL} = -K_p \simeq -\frac{4}{t_r}$

From the matrix $(A - DC)$ in (52), we calculate the parameters of the observer so as to have a common pole S_{ESO} of its characteristic polynomial:

$$\det(sI - (A - DC)) = s^2 + \beta_1.s + \beta_2 = (s - S_{ESO})^2 \quad (58)$$

From this equation, we deduce:

$$\beta_1 = -2.S_{ESO} \text{ and } \beta_2 = (S_{ESO})^2 \quad (59)$$

where $S_{ESO} \simeq (3 \ldots .10)S_{CL}$

B. Control of Rotor Currents by ADRC

From (27) and (28), the following expressions of rotor currents are deduced:

$$\frac{di_{rd}}{dt} = -\frac{R_r}{\sigma L_r} i_{rd} + \omega_r i_{rq} + \frac{1}{\sigma L_r} V_{rd} \quad (60)$$

$$\frac{di_{rq}}{dt} = -\frac{R_r}{\sigma L_r} i_{rq} - \omega_r i_{rd} - \omega_r \frac{L_m}{\sigma L_r L_s} \Phi_s + \frac{1}{\sigma L_r} V_{rq} \quad (61)$$

We put these expressions in the form:

$$\frac{di_{rd}}{dt} = f_d(i_{dr}, d, t) + b_0 u(t)$$

where

$$\begin{cases} f_d = -\frac{R_r}{\sigma L_r} i_{rd} + \omega_r i_{rq} + \left(\frac{1}{\sigma L_r} - b_0\right) V_{rd} \\ u = V_{rd} \quad , b_0 = \frac{1}{\sigma L_r} \end{cases} \quad (62)$$

$$\frac{di_{rq}}{dt} = f_q(i_{rq}, d, t) + b_0 u(t),$$

where:

$$\begin{cases} \mathrm{f_q} = -\frac{\mathrm{R_r}}{\sigma \mathrm{L_r}} \mathrm{i_{rq}} - \omega_\mathrm{r} \mathrm{i_{rd}} - \omega_\mathrm{r} \frac{\mathrm{L_m}}{\sigma \mathrm{L_r L_s}} \Phi_\mathrm{s} + (\frac{1}{\sigma \mathrm{L_r}} - \mathrm{b_0}) \mathrm{V_{rq}} \\ \mathrm{u} = \mathrm{V_{rq}} \quad , \mathrm{b_0} = \frac{1}{\sigma \mathrm{L_r}} \end{cases} \quad (63)$$

f_d and f_q are the total disturbance respectively affecting the rotor currents i_{rd} and i_{rq}. $u = V_{rd}$ and $u = V_{rq}$ are respectively the control inputs of the currents loops i_{rd} and i_{rq}. b_0 is the known part of the system parameters.

By choosing a suitable response time, we can easily determine the parameters k_p, β_1 and β_2 of the ADRC controllers, so that the rotor currents follow their reference i_{rd_ref} and i_{rq_ref} respectively given by (36) and (35).

C. Control of the DC Bus

The voltage U_{dc} across the capacitor C is given by (46).
We set $w = U_{dc}^2$, (46) can therefore be written as follows:

$$\frac{dW}{dt} = 3\frac{V_{sq}}{C} i_{qf} - 2\frac{\sqrt{W}}{C} i_{mr} \quad (64)$$

We put (64) in the canonical form of the ADRC regulator:

$$\frac{dW}{dt} = f(W, d, t) + b_0 . u$$

where

$$\begin{cases} f_w = -2\frac{\sqrt{W}}{C} i_{mr} + (3\frac{V_{sq}}{C} - b_0) i_{qf} \\ u = i_{qf} \quad , b_0 = 3\frac{V_{sq}}{C} \end{cases} \quad (65)$$

f_w represents the total disturbance, w and i_{qf} are respectively the output and the control input of the control loop of the voltage U_{dc}. b_0 is the known part of the system parameters.

We choose the controller parameters ADRC K_p , β_1 and β_2 , to maintain constant voltage DC bus.

D. Control Grid Side Converter

From (37) and (38), we determine the currents i_{df} and i_{qf} by the following expressions:

$$\frac{di_{df}}{dt} = \frac{1}{L_f} V_{sd} - \frac{R_f}{L_f} i_{df} - \omega_s i_{qf} - \frac{1}{L_f} V_{df} \quad (66)$$

$$\frac{di_{qf}}{dt} = \frac{1}{L_f} V_{sq} - \frac{R_f}{L_f} i_{qf} - \omega_s i_{df} - \frac{1}{L_f} V_{qf} \quad (67)$$

These equations can also be written as follows:

$$\frac{di_{df}}{dt} = f_{df}(i_{df}, d, t) + b_0 u(t),$$

where

$$\begin{cases} f_{df} = \frac{1}{L_f} V_{sd} - \frac{R_f}{L_f} i_{df} - \omega_s i_{qf} + (\frac{1}{L_f} - b_0) V_{df} \\ u = V_{df}, \quad b_0 = -\frac{1}{L_f} \end{cases} \quad (68)$$

$$\frac{di_{qf}}{dt} = f_{qf}(i_{qf}, d, t) + b_0 u(t),$$

where:

$$\begin{cases} f_{qf} = \frac{1}{L_f} V_{sq} - \frac{R_f}{L_f} i_{qf} - \omega_s i_{df} + (\frac{1}{L_f} - b_0) V_{qf} \\ u = V_{qf} \quad , b_0 = -\frac{1}{L_f} \end{cases} \quad (69)$$

f_{df} and f_{qf} represent the total disturbance. V_{df} and V_{qf} are respectively the control input of the control loops of currents i_{df} and i_{qf}. b_0 is the known part of the system parameters.

The reference current i_{df_ref} which can impose a zero grid side reactive power is deduced from (44):

$$i_{df\_ref} = \frac{2}{3}\frac{1}{V_{sq}} Q_{f\_ref} = 0 \quad (70)$$

The reference current i_{qf_ref} is deduced from (43) and (45):

$$i_{qf\_ref} = \frac{2}{3}\frac{i_{mf}}{V_{sq}} . U_{dc\_ref} \quad (71)$$

Similarly, we determine the ADRC controller parameters so that the currents i_{df} and i_{qf} follow their references.

VI. Simulation and Results

The overall model of the wind system using the doubly fed induction generator was simulated in Matlab/Simulink environment. The system parameters are given in the appendix.

To illustrate the performances of the ADRC command used to control this wind system, we conducted several tests in different conditions.

A. Test Tracking and Control

Fig. 9 shows the profile of the mechanical speed of the generator shaft driven in rotation by wind. The generator parameters are fixed and given in the appendix. Mechanical rotor speed varies between 1000 rpm and 1800 rpm.

Figs. 10-12 show that the rotor currents i_{rd} and i_{rq} perfectly follow their reference. The current i_{rq}, which controls the electromagnetic torque of the generator, varies in the same shape as the wind speed to extract the maximum power. The current i_{rd}, which controls reactive power Q_s, is kept constant to have a unity power factor on the stator side.

Figs. 13 and 14 show the total disturbances of the control loops of rotor currents. These disturbances are estimated and perfectly compensated by the regulator ADRC which allowed having a very good performance. We also note from these results, thanks to the ADRC, coupling between the two currents i_{rd} and i_{rq} disappeared.

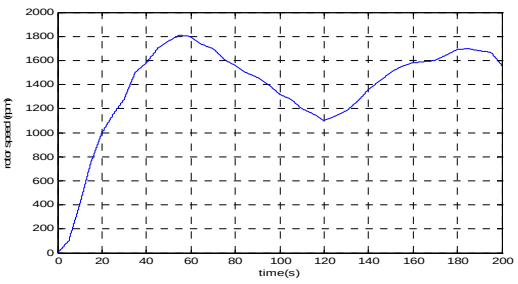

Fig. 9 Mechanical Rotor Speed

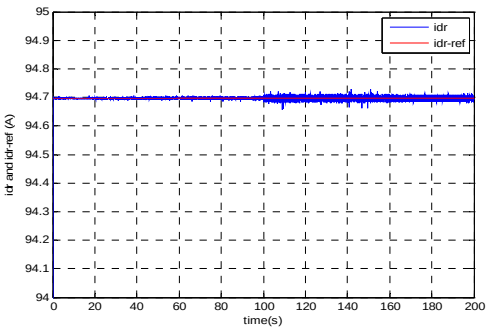

Fig. 10 Rotor Current i_{rd} and its Reference

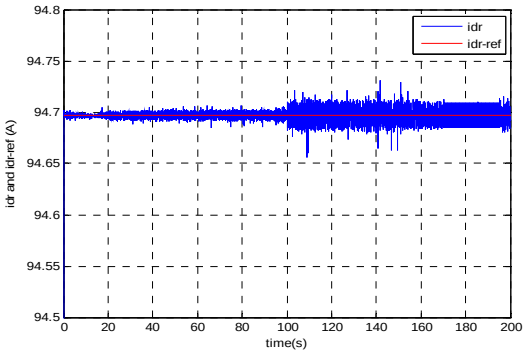

Fig. 11 Zoom on the Rotor Current i_{rd} and its Reference

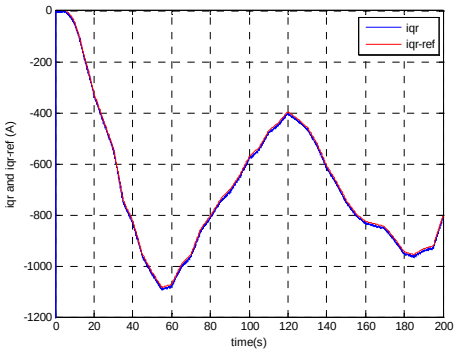

Fig. 12 Rotor Current i_{rq} and its Reference

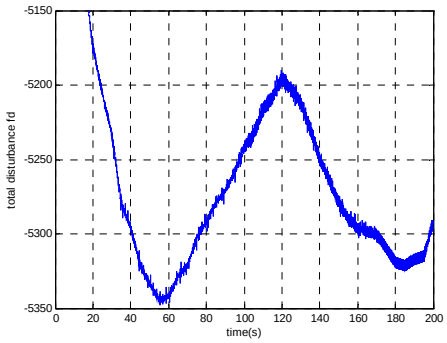

Fig. 13 Total Disturbance f_d

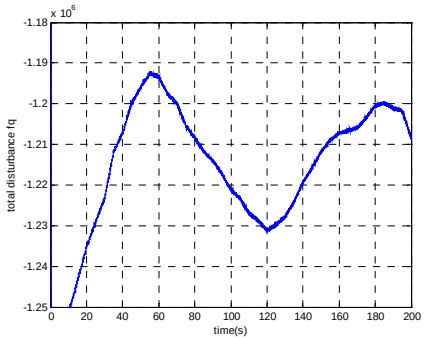

Fig. 14 Total Disturbance f_q

Figs. 15 and 16 show that the DC bus voltage U_{dc} is kept constant by the ADRC regulator. The fluctuations of such a voltage vis-à-vis the reference value of 700V are around 0.28%.

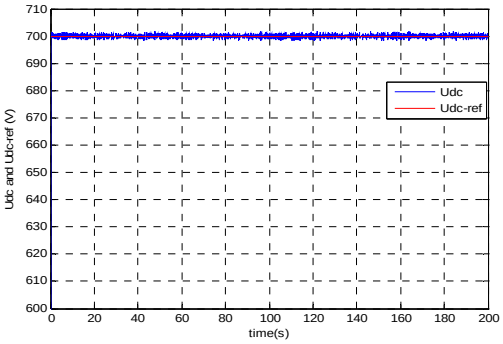

Fig. 15 Voltage U_{dc} and its Reference

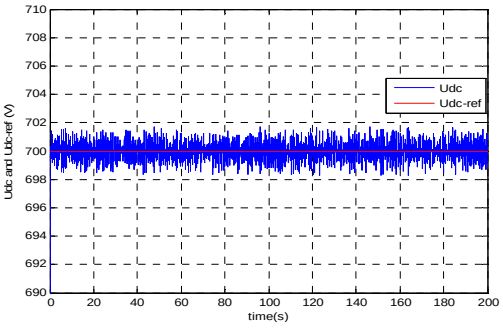

Fig. 16 Zoom on the Voltage U_{dc} and its Reference

Figs. 17-20 show the simulation results of currents i_{df} and i_{qf} of the filter (R_f, L_f), reactive and active power on grid side.

The current i_{df} perfectly follows its zero reference which enables to have a zero reactive power on grid side.

The current i_{qf} is maintained, by ADRC regulator, at its reference value, which allows having an evolution of the active power on grid side similar to wind profile.

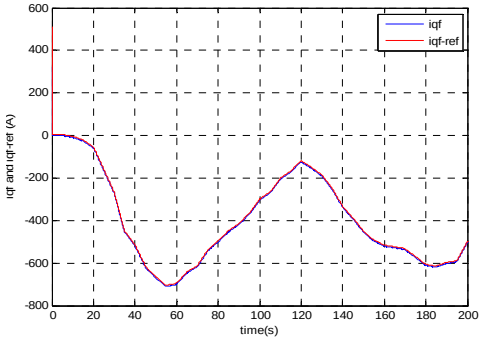

Fig. 17 Current i_{qf} and its Reference

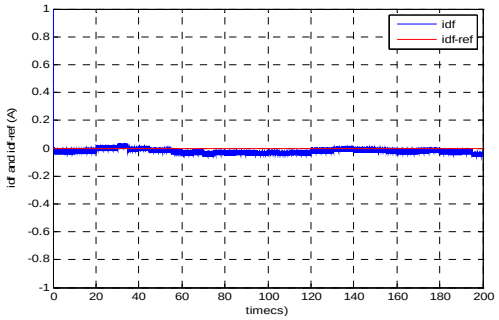

Fig. 18 Current i_{df} and its Reference

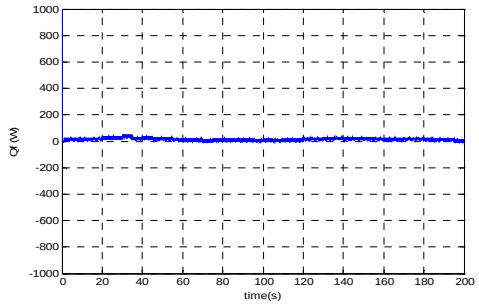

Fig. 19 Reactive Power Grid Side Q_f

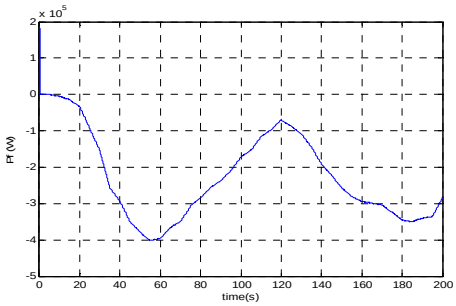

Fig. 20 Active power grid side P_f

B. Robustness Test

The test of robustness is to vary the parameters of the model of DFIG. In fact, the calculations of regulators are based on functions whose parameters are assumed to be fixed. However, in a real system, these parameters are subject to variations caused by different physical phenomena. Figs. 21-26 show the evolution of the current rotor after a 100% variation of the value of the rotor resistance R_r and a 150% rotor inductance L_r. These variations in R_r and L_r have almost no influence on the operation of the generator because ADRC regulators allow automatically compensate for the disturbance due to these variations. The tracking of setpoints is always ensured and the stability is not affected by variations of these parameters.

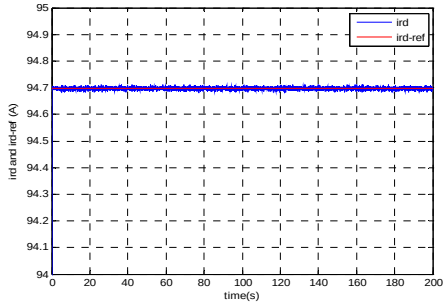

Fig. 21 Current i_{rd} and its Reference after a 100% variation of R_r

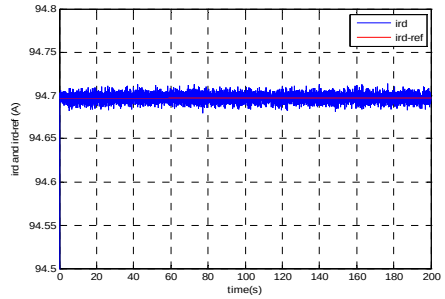

Fig. 22 Zoom on the Current i_{rd} and its Reference after a 100% variation of R_r

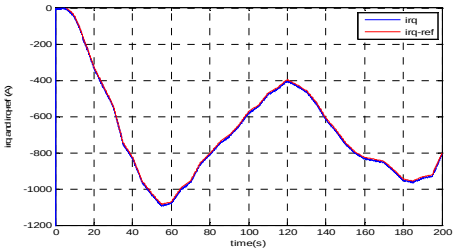

Fig. 23 Current i_{rq} and its Reference after a 100% variation of R_r

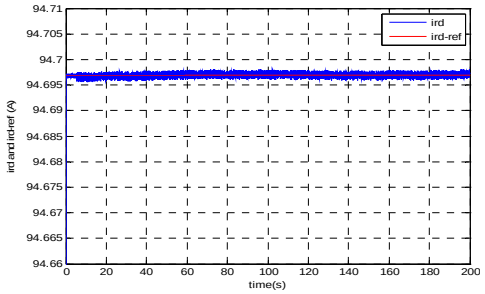

Fig. 24 Current i_{rd} and its Reference after a 150% variation of L_r

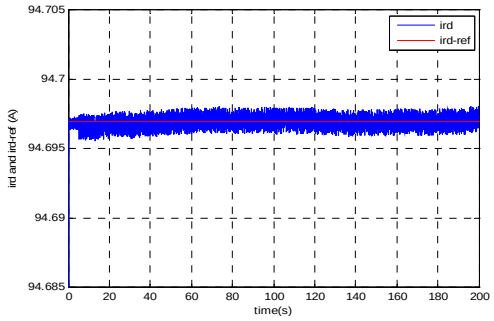

Fig. 25 Zoom on the Current i_{rd} and its Reference after a 150% variation of L_r

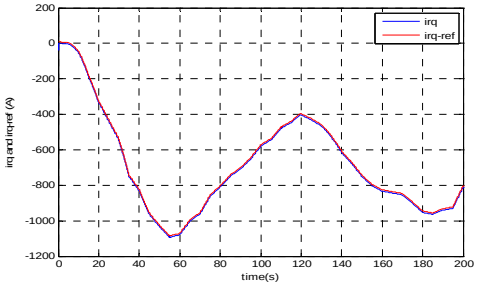

Fig. 26 Current i_{rq} and its Reference after a 150% variation of L_r

Figs. 27 and 28 show that after a 100% variation of the capacity of the DC bus, voltage U_{dc} always perfectly follows its setpoints and the voltage fluctuations do not exceed 0.4%.

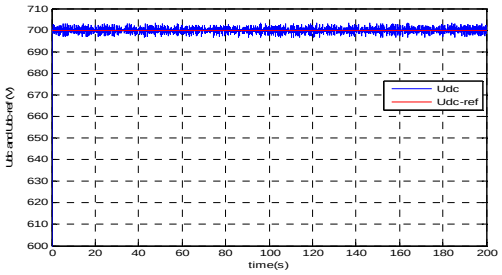

Fig. 27 Voltage U_{dc} and its Reference after a 100% variation of C

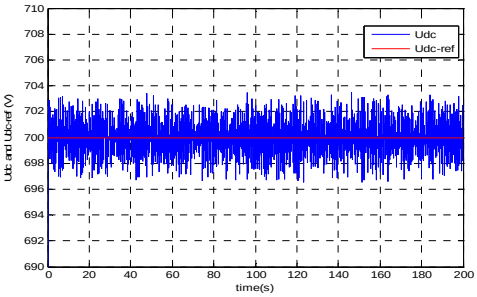

Fig. 28 Zoom on Voltage U_{dc} and its Reference after a 100% variation of C

Figs. 29 and 30 also show robustness of the ADRC regulators of the loops currents i_{df} and i_{qf}. The two currents perfectly follow their setpoints despite variation of the resistance R_f at 100%.

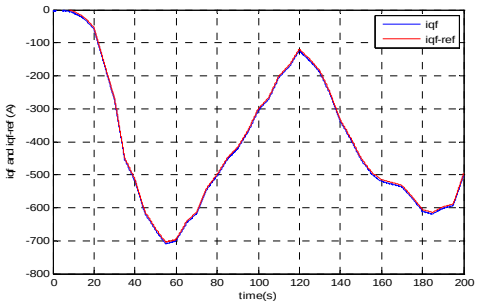

Fig. 29 Current i_{qf} and its Reference after a 100% variation of R_f.

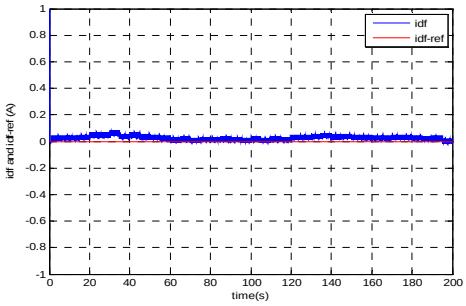

Fig. 30 Current i_{df} and its Reference after a 100% variation of R_f.

VII. Conclusion

This article has been devoted to modeling of a wind turbine based on a doubly fed induction generator, and developing a ADRC control which compensates the errors modeling and parametric variations of the system.

We could see through the results obtained in this paper, that the active disturbance rejection control is more efficient and allows for a better operation by eliminating the effect of external and internal disturbance, which represent the main problem in the electric power system.

The ADRC allows increasing system reliability and improving its energy efficiency.

Appendix

Doubly Fed Induction Generator Parameters:

Rated power: 300 KW
Stator and rotor resistance: $R_s = 8.9m\Omega$, $R_r = 13.7m\Omega$
Stator and rotor inductance: $L_s = 12.9mH$, $L_r = 12.7mH$
Mutual inductance: $L_m = 12.672mH$
Number of pole pairs: $p = 2$

Turbine Parameters:

Radius of the turbine: $R = 13.5m$
Gain multiplier: $G = 65$
Inertia total moment: $J = 10kg.m^2$
Air density: $\rho = 1.22kg/m^2$
Coefficient of viscous friction: $f = 0.0001$
Optimal tip speed ratio: $\lambda_{opt} = 8.1$
Maximal power coefficient: $C_{pmax} = 0.45$

Connecting to the Grid Parameters:

Filter inductance: $L_f = 2.5mH$
Filter resistance: $R_f = 75m\Omega$
DC link capacity: $C = 4400\mu F$

Adrc Controller Parameters

Rotor currents controller gain: $K_{p\_r} = 133.33$
Rotor currents parameter: $b_{r0} = 4069.3$
Observation parameters of the loop currents rotor: $\beta_{1r} = 1066.7$, $\beta_{2r} = 284.44e^3$
Filter currents controller gain: $K_{p\_f} = 200$
Filter currents parameter: $b_{f0} = -400$
Observation parameters of the loop currents filter: $\beta_{1f} = 2000$, $\beta_{2f} = 10^6$
DC link voltage controller gain: $K_{p\_c} = 400$
DC link voltage parameter: $b_{c0} = 385e^3$
Observation parameters of the loop DC link voltage: $\beta_{1c} = 3200$, $\beta_{2c} = 256e^4$

REFERENCES

[1] Fredo, B., Marco, L. and Ke, M. Power Electronics Converters for Wind turbine Systems, IEEE Transaction on industry applications, vol. 48, No. 2, March/April 2012.
[2] Tapia, A., Tapia, G., Ostolaza, J.X. and Saenz, J.R. Modeling and control of a wind turbine driven doubly fed induction generator, IEEE Transactions on Energy conversion, vol. 18, No. 2, June 2003.
[3] Han, Jingqing. From PID to Active disturbance rejection Control, IEEE Transaction on industrial electronics, vol.56, No.3, March 2009.
[4] Xu, L. and Cartwright, P. Direct active and reactive power control of DFIG for wind energy generation, IEEE Transactions on Energy conversion, vol. 21, No. 2, Sept 2006.
[5] Gernot, H. A Simulative Study on Active Disturbance Rejection Control (ADRC) as a Control Tool for Practioners, Electronics 2013,2,246-279;doi:10.3390/electronics2030246.
[6] Pablo, L. and Julio, U. Doubly Fed Induction Generator Model for transient Stability Analysis, IEEE Transaction on energy conversion, vol. 20, No. 2, June 2005.
[7] Betran, B., Ahmed-ali, T., and Benbouzid, M.E.H, Sliding Mode Power Control of Variable Speed Wind Energy Conversion systems, IEEE Transaction on energy conversion, vol. 23, No. 2, June 2008.
[8] Oscar, B. Sliding Mode Control strategy for Wind Turbine Power Maximization, Energies 2012, 5, 2310-2330; doi:10..3390/en5072310.
[9] Muller, S., Diecke, M., and Doncher, R.W, Doubly Fed Induction Generator Systems for Wind Turbines, IEEE Industry Applications Magazine, vol. 8, Issue 3, May/June 2002.
[10] Zheng, O., On Active Disturbance Rejection Control: Stability analysis and Applications in Disturbance Decoupling Control, Ph.D. Dissertation, Dept of Elect. Comp. Eng., Cleveland State University, Cleveland, USA, July 2009.
[11] Zheng, Q. and Gao, Z. On Practical Applications of Active Disturbance rejection Control, Proceeding of the 29th chinese conference, July 29-31, 2010, Beijing, China.
[12] Wankun, Z., Shao, S. and Gao, Z., A Stability Study of the active disturbance rejection Control Problem by a Singular Perturbation approach, Applied Mathematical sciences, vol. 3, No. 10, 491-508.
[13] Jingqing, H., Auto-Disturbance Rejection Control and its Applications, Control decision, vol. 13, No. 1, 1998, pp. 19-23.
[14] GHENNAM, T., 2011, Supervision d'une ferme éolienne pour son integration dans la gestion d'un réseau électrique, Apport des convertisseurs multi niveaux au réglage des éoliennes à base de machine asynchrone à double alimentation, Thèse de doctorat, No d'ordre. 162, Ecole Centrale de Lille.
[15] Eftichios, K. and Kostas, K., Design of a maximum power tracking system for wind-energy-conversion applications, IEEE Transaction on industrial electronics, vol. 53, No. 2, pp. 486-494, April 2006.

R.Chakib was born in Rabat, in 1973 Morocco. He received the Engineer Degree in Electrical Engineering, from Ecole Nationale Supérieure d'Electricité et de Mécanique (ENSEM), Casablanca, Morocco, in 1997. He is currently preparing a PhD thesis in the department of Electrical Engineering of Mohammedia School of Engineers (EMI), university Mohamed V, Rabat, Morocco.

His research areas include renewable energy, machine control and electrical systems.

A.Essadki is currently a Professor and university research professor at the electrical engineering department of ENSET, Mohammed V Souissi university Morocco**.** In 2000, he received his PhD degree from Mohammedia Engineering School (EMI), Morocco. From 1990 to 1993, he pursued his master program at UQTR university, Quebec Canada, respectively, all in electrical engineering. His current research interests include renewable energy, motor drives and power system. Dr ESSADKI is a member of RGE Lab in research group Leader

M.Cherkaoui was born in Marrakech, Morocco in 1954. He received the Engineer Degree in Electrical Engineering, from Mohammedia Engineering School (EMI), Rabat, Morocco, in 1979. He received his PhD degree from Institut National Polytechnique de Lorraine, Nancy, France in 1985. In 1986, he joined the university of Caddi Ayyad in Merrakech as a researcher professor. In 1995, he moves then to the Mohammedia Engineering School (EMI), Rabat, as a professor of higher education and head of Electrical engineering department.

Prof. Cherkaoui is a director of the research laboratory in electrical power and control of the Mohammedia engineering school (EMI), Rabat,Morocco. He is also an expert with Moroccan ministry for higher education and with industrialists to matters related to the energetic efficiency.His main research interests are renewable energy and control of electrical systems.